# CMS Physics Analysis Summary

2008/03/19

# Search for Heavy Stable Charged Particles with 100 $pb^{-1}$ and 1 $fb^{-1}$ in the CMS experiment

The CMS Collaboration

## Abstract

The CMS detector can be used to search for Heavy Stable Charged Particles (HSCPs) which might signal physics beyond the Standard Model. Such particles can be distinguished from Standard Model particles by exploiting their unique signature: a low velocity, $\beta$, associated with a high momentum of order a few hundred GeV/c. In this note four models predicting different types of HSCP are described and used as benchmarks for a proposed search strategy. Two techniques to measure $\beta$ of such particles using the Silicon Tracker and the Barrel Muon Drift Tube detectors are reviewed, and results based on full simulation of the CMS detector are presented. These include the expected performance and resolutions which could be obtained using the first data from CMS at the LHC. The HSCP mass regions explored for integrated luminosities of 100 $pb^{-1}$ and 1 $fb^{-1}$ are shown.

# Introduction

In this note we investigate the possibility of searching for Heavy Stable Charged Particles (HSCPs) using the CMS detector. The emphasis is on discoveries which could be made with the first data collected by the experiment after the turn-on of the Large Hadron Collider (LHC). Four specific models involving HSCPs are studied using the full CMS simulation. The parameters used in the models lead to HSCPs of different masses.
The key element of this analysis is the measurement of the velocity $\beta$ of the HSCP. Two techniques to measure $\beta$ have been developed, one based on time-of-flight measurement by the Drift Tube subsystem of the muon detector, and the other using specific ionization in the central Tracker detector.
Some possible analysis strategies and candidate event selections are discussed and the results expected from the first data collected by CMS are presented.

# 1 Models and sample generation

HSCPs arise in models in which one or more new states exist and which carry a new conserved, or almost conserved, global quantum number. Supersymmetry with R-parity and extra dimensions with KK-parity provide examples of such models. A review of models with HSCPs can be found in [1]. The lightest of the new states will be stable, due to the conservation of this new parity and depending on quantum numbers, mass spectra, and interaction strengths, one or more heavier states may also be stable or metastable. In general, electrically-charged stable states are incompatible with the dark matter problem [1], and colored particles are strongly constrained. For this reason, models that address the dark-matter problem include, in general, a stable uncharged weakly interacting massive particle. They may also have, in addition, one or more higher-lying metastable charged states.

HSCPs could be produced at the LHC as a result of direct pair-production processes or as final products of the decay chain of heavier exotic particles. HSCPs with strong charge will hadronize and form mesons, baryons or glueballs. These hadronized states are generically called R-hadrons.

Four benchmark models including HSCPs have been considered in this document. Two of them predict the existence of lepton-like HSCPs whereas the other two include different species of R-hadrons.

Quasi-stable sleptons (stau) are predicted in the framework of Gauge Mediated Supersymmetry Breaking (GMSB) [2] supersymmetric models. Production of the stau at the LHC can proceed directly via a virtual photon or $Z$ or via production of heavier supersymmetric particles (mainly squarks and gluino pairs). In the latter case, which is in general dominant due to the electroweak nature of the direct production process, one or more $\tilde{\tau}_1$ will appear in the final state as final products of the decay chain of the sparticles. The particle mass spectrum and the decay table were produced with the program ISASUGRA [3] version 7.69. The model selected is the minimal GMSB (mGMSB) and two benchmark points on the SPS line 7 [4] were chosen. The parameter values corresponding to these two points are as follows:

- $\tilde{\tau}_1$ (156) : $N = 3$, $\Lambda = 50000$ GeV, $M = 100000$ GeV, $\tan\beta = 10$, $sign(\mu) = 1$, $c_{grav} = 10000$
- $\tilde{\tau}_1$ (247) : $N = 3$, $\Lambda = 80000$ GeV, $M = 160000$ GeV, $\tan\beta = 10$, $sign(\mu) = 1$, $c_{grav} = 10000$

The corresponding $\tilde{\tau}_1$ masses are 155.8 and 247 GeV, and the squark/gluino masses are of order

1.1 TeV and 1.7 TeV respectively. At both points the squark and gluino production cross sections are between one and two orders of magnitude higher than that of direct $\tilde{\tau}_1$ pair production.

Quasi-stable sleptons are also predicted by the Universal Extra Dimensions model [5] (UED). According to UED, all Standard Model (SM) particles uniformly propagate in extra dimensions of size $R^{-1} \sim$ TeV. UED models predict that for all SM particles there exist corresponding so-called Kaluza-Klein (KK) states in extra dimensions, which have the same quantum numbers and spins as their SM partners. The dominant mode for KK lepton production in p-p collisions is direct pair production. At the LHC the cross section of $pp \rightarrow \tau_R^1, \bar{\tau}_R^1$ is about 20 fb for 300 GeV KK $\tau$, where $\tau_R^1, \bar{\tau}_R^1$ are KK $\tau$ and anti-KK $\tau$ respectively. In principle, the right-handed KK $\tau$ can also be produced from cascade decay of KK $Z$ boson or level 2 KK $\tau$s. But the cross section of these processes is $\sim 5$ fb. So in this study we mainly focus on the direct pair production of right-handed KK $\tau$.

A long-lived gluino ($\tilde{g}$ ) can occur in the so-called split SUSY [6] scenario, where all the SUSY scalar particles have very large masses (many TeV), while only the gaugino and the higgsino masses are still around the weak scale (of order TeV). The most distinctive feature of the theory is that the gluino becomes metastable [7], because it can only decay via virtual squarks. Depending on the parameters of the model, the $\tilde{g}$ mass can be essentially any value between several hundred GeV/$c^2$ and the order of several TeV/$c^2$.
In the MSSM framework a scenario with a light stop next-to-lightest SUSY particle is motivated by electroweak baryogenesis[8]. In this scenario non-universal squark mass terms are used to arrange a small mass difference between the $\tilde{t}_1$ and the lightest SUSY particle (LSP), while the lightest chargino is kept too heavy for the decay $\tilde{t}_1 \rightarrow b\chi_1^+$ to occur. In this case, only the radiative process $\tilde{t}_1 \rightarrow c\chi_1^0$ is open, and the $\tilde{t}_1$ can be quite long-lived.
Another interesting scenario in which a stop would be stable (and indeed the LSP) can be obtained by breaking the electroweak symmetry and supersymmetry by a compact extra dimension [9]. In this case the favoured stop mass range is between 130 and 800 GeV.

After production, both the $\tilde{g}$ and $\tilde{t}_1$ hadronize to a metastable particle by combining with light quarks or gluons. Such a state is generically called an R-hadron and could be an R-baryon $\tilde{g}qqq$ or $\tilde{g}\bar{q}\bar{q}\bar{q}$, R-meson $\tilde{g}q\bar{q}$ or R-gluonball $\tilde{g}g$. The fraction of produced R-gluonballs is an unknown parameter of the underlying hadronization model. This parameter affects the fraction of R-hadrons that are neutral at production.
In this study, hadronization of $\tilde{g}$ and $\tilde{t}_1$ was performed with PYTHIA dedicated routines. In the $\tilde{g}$ case, the fraction of produced R-gluonballs was arbitrarily set to 0.1.

## 2 Trigger

At trigger level, a lepton-like HSCP has a high probability of being reconstructed as a muon. Reconstruction can fail, however, if the HSCP is too slow. In this case it will reach the muon system out of time with respect to typical relativistic muons and therefore would either be reconstructed in the wrong bunch crossing or fail to be reconstructed at all because of quality cuts imposed by the Level-1 Trigger (L1) or High Level Trigger (HLT) algorithms. In the case of R-hadrons, reconstruction in the muon system is expected to be even more problematic due to the charge-flipping effect, especially in the iron yoke or calorimeters. R-hadrons are indeed hadronically interacting with matter, when those interactions occur the quarks bound to the $\tilde{g}$ or $\tilde{t}_1$ can change therefore the total charge of the hadron is modified [10] [11]. Matching or fitting of the individual measurements in the muon stations could fail due to the change in the

| Data Sample | Cross section (pb) | HSCP in $\|\eta\| < 2.4$ (%) | HSCP in $\|\eta\| < 0.9$(%) |
|---|---|---|---|
| $\tilde{\tau}_1$ (156 GeV) | 1.19 | 97.6 | 72.6 |
| $\tilde{\tau}_1$ (247 GeV) | 0.097 | 97.5 | 70.9 |
| KK tau (300 GeV) | 0.020 | 84.7 | 40.9 |
| $\tilde{g}$ (200 GeV) | $2.2 \times 10^3$ | 89.7 | 47.4 |
| $\tilde{g}$ (300 GeV) | 100 | 91.7 | 50.0 |
| $\tilde{g}$ (600 GeV) | 5.00 | 93.7 | 55.5 |
| $\tilde{g}$ (900 GeV) | 0.46 | 92.6 | 57.7 |
| $\tilde{g}$ (1200 GeV) | $61 \times 10^{-3}$ | 91.4 | 53.9 |
| $\tilde{g}$ (1500 GeV) | $10 \times 10^{-3}$ | 90.4 | 55.8 |
| $\tilde{t}_1$ (130 GeV) | $1.11 \times 10^3$ | 87.8 | 43.1 |
| $\tilde{t}_1$ (200 GeV) | $1.77 \times 10^2$ | 90.9 | 47.3 |
| $\tilde{t}_1$ (300 GeV) | 27.4 | 92.8 | 50.4 |
| $\tilde{t}_1$ (500 GeV) | 1.27 | 95.3 | 54.7 |
| $\tilde{t}_1$ (800 GeV) | $7.81 \times 10^{-2}$ | 96.9 | 61.9 |

Table 1: First two columns show the data samples and their cross sections. The last two columns contain the percentage of events for each sample having at least one HSCP in $|\eta| < 2.4$ and $|\eta| < 0.9$, respectively.

bending of the R-hadron track or because of absence of measurements in the stations where the R-hadron is electrically neutral. It can also happen that an R-hadron appears neutral in the tracker, but charged in the muon system. In this case there can be no match between tracks measured in the Muon and in the inner tracker [12], Finally, the R-hadron energy deposition in the calorimeters may be sufficient for muon reconstruction to fail the isolation criteria.

HSCPs can also give rise to a sizeable missing energy, unless back-to-back pair production cancels out individual contributions. The missing energy trigger neither suffers from the timing issues described above, nor does it depend on whether HSCPs are reconstructed successfully as muons because muons are not expected to be considered in the missing energy estimate at trigger level. The missing energy trigger, as well as other calorimeter-based triggers (e.g. $E_t^{SUM}$, jets), could become very efficient for HSCP events due to model-specific features like the underlying production mechanism or the nature of the heavy particle itself. Table 2 summarises the High Level Trigger efficiencies expected for low luminosity running of LHC.

## 3 Beta Measurements

The identification of a HSCP relies on the fact that it can be slow ($v < c$) but with high momentum ($p \gtrsim 100$ GeV). It is then possible to measure the mass of a particle if both $\beta$ and the momentum are measured.

Two approaches have been followed, one based on time-of-flight (TOF) measured with the Drift Tube (DT) detector and one based on specific ionization in the Tracker.

In each wheel of the barrel of CMS there are four muon stations. Each station except the outermost contains three super-layers (SL), each of four DT layers. The outermost station contains two SL. Two of the SL measure the $r - \phi$ coordinate and one measures the $z$ coordinate (the out-

| HLT Trigger Path | 1MuonNonIso | | 1MET | | 1SumET | | 1Jet | | **Previous** | **Others** |
|---|---|---|---|---|---|---|---|---|---|---|
| Efficiency (%) | Abs | Inc | Abs | Inc | Abs | Inc | Abs | Inc | Abs | Inc |
| $\tilde{\tau}_1$ 156 (GeV) | 96.8 | **96.8** | 84.1 | **1.9** | 91.3 | **0.5** | 74.9 | **0.0** | **99.2** | **0.2** |
| $\tilde{\tau}_1$ 247 (GeV) | 96.8 | **96.8** | 81.5 | **2.1** | 87.4 | **0.6** | 63.5 | **0.0** | **99.5** | **0.1** |
| tau 300 (GeV) | 75.2 | **75.2** | 7.8 | **2.2** | 7.9 | **1.2** | 2.1 | **0.0** | **78.6** | **4.4** |
| $\tilde{t}_1$ 130 (GeV) | 21.9 | **21.9** | 18.1 | **12.5** | 17.3 | **3.2** | 3.9 | **0.0** | **37.6** | **2.1** |
| $\tilde{t}_1$ 200 (GeV) | 23.7 | **23.7** | 26.0 | **18.1** | 25.1 | **4.1** | 7.0 | **0.0** | **45.9** | **3.4** |
| $\tilde{t}_1$ 300 (GeV) | 23.5 | **23.5** | 33.4 | **24.4** | 35.7 | **5.8** | 10.8 | **0.0** | **53.7** | **4.0** |
| $\tilde{t}_1$ 500 (GeV) | 23.4 | **23.4** | 39.3 | **29.6** | 48.3 | **8.4** | 17.3 | **0.0** | **61.4** | **5.6** |
| $\tilde{t}_1$ 800 (GeV) | 22.0 | **22.0** | 44.8 | **34.5** | 62.9 | **14.0** | 21.7 | **0.0** | **70.5** | **6.6** |
| $\tilde{g}$ 200 (GeV) | 22.4 | **22.4** | 28.5 | **21.3** | 44.6 | **13.6** | 9.8 | **0.0** | **57.3** | **1.8** |
| $\tilde{g}$ 300 (GeV) | 22.6 | **22.6** | 35.3 | **26.7** | 58.0 | **17.8** | 14.0 | **0.0** | **67.0** | **2.1** |
| $\tilde{g}$ 600 (GeV) | 21.3 | **21.3** | 47.1 | **36.1** | 83.2 | **27.9** | 23.1 | **0.0** | **85.4** | **1.3** |
| $\tilde{g}$ 900 (GeV) | 16.6 | **16.6** | 49.5 | **40.0** | 92.4 | **36.3** | 29.2 | **0.0** | **92.9** | **1.0** |
| $\tilde{g}$ 1200 (GeV) | 11.7 | **11.7** | 55.6 | **47.6** | 95.0 | **36.0** | 34.0 | **0.0** | **95.3** | **0.8** |
| $\tilde{g}$ 1500 (GeV) | 11.3 | **11.3** | 56.2 | **49.1** | 96.0 | **35.7** | 45.2 | **0.0** | **96.1** | **0.2** |

Table 2: HLT efficiency for all simulated data samples. Only events with at least one HSCP in $|\eta| < 2.4$ are considered. The incremental efficiency reported in each column is relative to the paths in the columns on the left. The last column in the table reports the total efficiency obtained with the four paths listed in the table as well as the incremental efficiency of all the HLT paths not listed in the table relative to those present in the table.

ermost station lacks a $z$ SL). Drift Tubes are 2-3 m long, 12 mm high and 42 mm wide. Maximal drift distance to the sensitive wire is 20 mm. Because tubes in consecutive layers are staggered by half a tube, a typical track passes alternatively on the left and right side of the sensitive wires in consecutive layers.

Particles travelling slower than a higly relativistic muon arrive at the muon system with a time delay. The reconstructed hits for each tube will be shifted with respect to its real position. The result will be that the right and left hits produce a zig-zag pattern instead of a straight line.
It is possible to compute the particle time delay with respect to a muon, and so the total time of flight, from the position of these hits. The only requirement is that at least three hits, with at least one right and one left, be present in the given SL, and that the track is registered by a perpendicular layer in the same muon station.

The CMS silicon tracker is able to measure the energy deposited by each hit (analog readout). After proper normalization this can be transformed into a $\frac{dE}{dx}$ measurement.
A track is typically associated with $\sim 15$ hits thus giving a good estimate of the Most Probable Value (MPV) $\frac{dE}{dx}$. Since the ionization MPV depends on the $\beta$ of the particle with an approximately $\beta^{-2}$ dependence in the region $0.1 < \beta < 0.8 \div 0.9$, we measure $\beta$ from $\frac{dE}{dx}$.

$$\beta^{-1} = \sqrt{K\frac{dE}{dx}}, \tag{1}$$

where the constant factor $K$ can be obtained directly from data using low momentum protons and kaons. The protons can also be used to check the linarity of the tracker response as a function of the deposited energy.

The resolution of $\beta$ for standard model particles can be evaluated directly from data in both

cases. The tails of the resolution functions for each measurement must also be evaluated in a robust way using data so that any observed excess can be reliably considered as evidence for a signal. For this purpose $Z \rightarrow \mu\mu$ events can be selected, using Z mass constraint, and can be used to directly measure the tails on real data.

# 4 Selection and results with early data

In order to maximize the background rejection, we use a combined selection based on the two measurements of $\beta$ in the DT and Tracker. We also investigate a standalone selection based only on tracker measurements. The combined selection is expected to maximize the S/B ratio, in effect reducing the background to a negligible level without significant loss of signal. The usage of tracker reduces to a negligible level the background due to cosmic muons or to muons from different bunch crossing.

## 4.1 Combined selection

The first step in the selection process is to associate the candidate HSCP measured in the muon system with the one measured in the tracker. All the tracks reconstructed in the muon system with $p_T > 30$ GeV are considered as HSCP candidates, while for the tracker candidates a preselection is applied:

- $p_T > 30$ GeV
- $\beta_{tk} < 0.9$
- number of $\frac{dE}{dx} hits >= 9$
- $\frac{\chi^2}{ndof} < 5$

The two collections are associated by geometric and momentum compatibility, according to the following requirements:

- $\Delta(1/p_T) < 0.005\ \text{GeV}^{-1}$
- $\Delta R = \sqrt{\Delta\eta^2 + \Delta\varphi^2} < 0.1$.

If more than one match satisfies the above criteria, the match with smallest $\Delta R$ is taken.
Figure 1 shows the distribution of $\beta_{Tk}^{-1}$ vs $\beta_{Dt}^{-1}$ for background and signal events after matching. For signal events, the two measurements are clearly correlated. Correlation between measurements for the background is not present. Therefore, for the combined DT/Tracker analysis, it is possible to require that the two measurements are compatible and/or that both are above a threshold.

A clean signal region can be defined by applying cuts on both $\beta$ measurements and some simple quality cuts:

- $\beta_{DT} < 0.80$ and $\sigma_{\beta^{-1}} < 0.1$
- $\beta_{Tk} < 0.80$
- $m_{avg} > 100$ GeV

where $m_{avg}$ is the mass obtained averaging the $\beta$ measurements from the two subdetectors.
The efficiency of the first two cuts can be measured independently, and it can be assumed that there is no correlation between the two measurements for the background. This hypothesis can be directly verified on data. These two cuts alone provide a rejection of $\sim 10^{-7}$, i.e. $\sim 0.1$ events are expected in 1M events ($\sim 1\ \text{fb}^{-1}$ for the Muon Primary Dataset after a preliminary

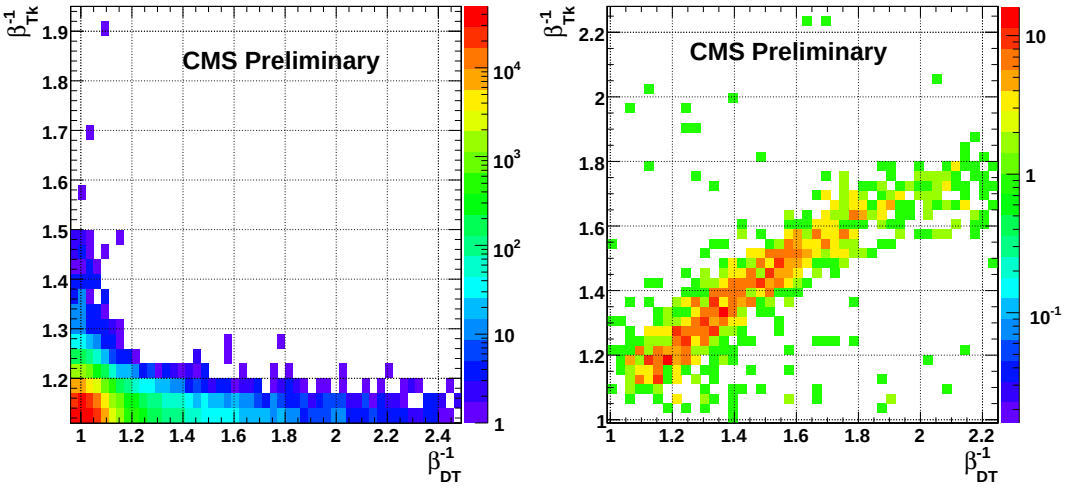


Figure 1: Distribution of $\beta_{Tk}^{-1}$ versus $\beta_{DT}^{-1}$ for background (left) and for the signal sample $\tilde{t}_1$ with mass 500 GeV (right).

selection). No background events pass the above selection in a fully-simulated MC sample corresponding to $\sim 1$ fb$^{-1}$. The efficiency of the above selection for signal samples is reported in Table 3.

In the case where the tails of the two $\beta$ distributions are higher when they are measured on data than what is expected from simulation, a tighter selection can be used. The goal is to have less than one background event expected for 1 fb$^{-1}$. Several additional cuts can be used which drastically reduce the background, but have small effects on the signal. They cannot be properly investigated on the background for the available statistics since the simple selection proposed above leaves no events.

## 4.2 Tracker standalone selection

A standalone selection using only the tracker for the $\beta$ measurement is the following:

- 1 reconstructed muon with $p_T > 100$ GeV
- $\beta_{tk} < 0.8$.

The muon system is still used but no time-of-flight information is extracted from it. This analysis has been tested on a sample of events expected to be selected by the muon trigger and corresponding to about 1 fb$^{-1}$ of integrated luminosity. The resulting number of selected events is reported in Table 4. The efficiency on signal samples is slightly higher than that of the combined analysis given that the DT coverage, which is not required for the standalone selection, is limited to the barrel region of CMS.

## 4.3 Systematic uncertainty

The first source of systematic uncertainty is the trigger efficiency for late particles. The final muon trigger settings for time gates and synchronization can change the efficiency for triggering on a late particle in the correct bunch crossing. This can easily change the trigger efficiency by 50% and can shift the spectrum of the recorded HSCP towards higher values of $\beta$, further

| Sample (mass) | $\beta_{DT} < 0.85$ $\sigma_{\beta^{-1}} < 0.10$ | $\beta_{DT} < 0.80$ $\sigma_{\beta^{-1}} < 0.10$ | $\beta_{Tk} < 0.80$ | $\beta_{DT} < 0.80$ and $\beta_{Tk} < 0.80$ $\sigma_{\beta^{-1}} < 0.10$ | $\sigma_{\beta^{-1}} < 0.07$ |
|---|---|---|---|---|---|
| $\tilde{g}$ (200 GeV) | 0.079 | 0.069 | 0.130 | **0.062** | 0.053 |
| $\tilde{g}$ (300 GeV) | 0.097 | 0.088 | 0.172 | **0.081** | 0.069 |
| $\tilde{g}$ (600 GeV) | 0.117 | 0.109 | 0.235 | **0.103** | 0.088 |
| $\tilde{g}$ (900 GeV) | 0.141 | 0.136 | 0.255 | **0.126** | 0.110 |
| $\tilde{g}$ (1200 GeV) | 0.128 | 0.126 | 0.240 | **0.111** | 0.090 |
| $\tilde{g}$ (1500 GeV) | 0.137 | 0.136 | 0.285 | **0.117** | 0.102 |
| KK tau (300 GeV) | 0.342 | 0.287 | 0.465 | **0.264** | 0.239 |
| $\tilde{t}_1$ (130 GeV) | 0.079 | 0.067 | 0.116 | **0.060** | 0.053 |
| $\tilde{t}_1$ (200 GeV) | 0.098 | 0.083 | 0.159 | **0.078** | 0.067 |
| $\tilde{t}_1$ (300 GeV) | 0.122 | 0.108 | 0.205 | **0.101** | 0.088 |
| $\tilde{t}_1$ (500 GeV) | 0.145 | 0.130 | 0.258 | **0.119** | 0.105 |
| $\tilde{t}_1$ (800 GeV) | 0.170 | 0.156 | 0.305 | **0.148** | 0.129 |
| $\tilde{\tau}_1$ (156 GeV) | 0.332 | 0.236 | 0.331 | **0.199** | 0.182 |
| $\tilde{\tau}_1$ (247 GeV) | 0.452 | 0.347 | 0.491 | **0.298** | 0.269 |

Table 3: HSCP selection efficiencies for reconstructed masses $m > 100$ GeV. The last column shows the efficiency with a tighter cut on the $\beta_{DT}$ error (as a reference). The selection efficiency used in the next section is that quoted in bold in the fifth column.

| Primary Dataset | $m > 100$ GeV | $m > 200$ GeV | $m > 400$ GeV |
|---|---|---|---|
| Muon | 681 | 318 | 84 |

Table 4: Number of selected background events expected in 1fb$^{-1}$ with tracker standalone selection.

reducing the final efficiency. It should be noted that the MET trigger does not suffer this problem and can in principle recover some of the lost events.

This loss of efficiency has the same effect as an uncertainty in the signal cross section, assuming that some slow particles have caused a trigger. Even if it affects the integrated luminosity needed for discovery or exclusion, it does not change the background behavior.

Another source of systematic uncertainty comes from the evaluation of the tails of the $\beta$ distributions as measured with the tracker and with the DT. In the following calculations, we assume that the number of background events populating those tails is predicted by the simulation. Nevertheless those tails can be directly measured on data at the start of data taking. Some preliminary investigations have already started using the Tracker Integration Facility data (5M cosmics) to evaluate the $\frac{dE}{dx}$ distribution and the DT commissioning data to evaluate the time resolution [13].

The effect of initial detector misalignment is taken into account in the background simulation. The reconstruction is performed with the so called 10 pb$^{-1}$ conditions. This scenario assumes that the detector has been realigned by using the first 10 pb$^{-1}$ of integrated luminosity, which will probably be the best available information for a first processing of the first 100 pb$^{-1}$ of data. An improvement is expected when processing the first 1 fb$^{-1}$ since the detector alignment

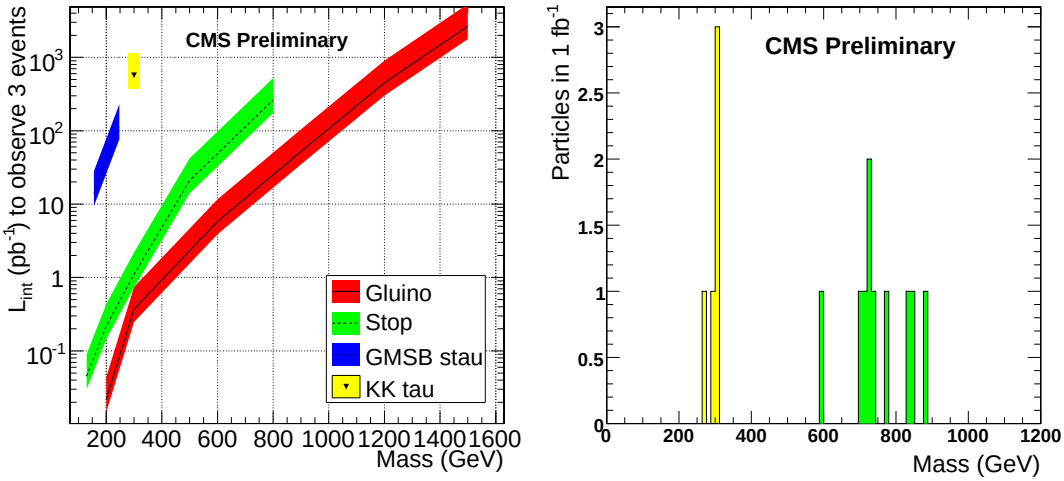


Figure 2: The left plot shows the integrated luminosity ($pb^{-1}$) needed for 3 events, for the four signal models (gluino full circles, stop full squares, KK tau empty circles, stau empty squares) as a function of HSCP mass. The right plot shows the reconstructed mass distribution with 1 $fb^{-1}$ for two of the lowest cross section samples (300 GeV KK tau and 800 GeV stop).

would be recomputed using more data.

## 4.4 Discovery and exclusion

In the following, we compute the luminosity needed to observe 3 events in the signal region for different models as an estimate for the integrated luminosity needed for exclusion/discovery when no background events are expected. If an excess is observed it is also possible to perform several cross checks. First, one can check the distribution of the reconstructed mass (as shown in the right plot of Figure 4.4).

The Poisson probability to observe no events when 3 are expected is 5%. Therefore, we can claim a 95% C.L. exclusion if no events are observed when the luminosity for 3 events has been accumulated.

Figure 4.4 shows the required luminosity to select three Heavy Stable Charged Particles for different signal samples. The error bars correspond to a systematic uncertainty of 50% on the trigger efficiency.

For the tracker standalone analysis, the luminosity needed for a 95% C.L. exclusion has been computed with a likelihood ratio method [14], and the result is shown in Figure 4.4.

## 4.5 Conclusions

Heavy Stable Charged Particles can be discovered with early data for different models and in different mass regions. The stable gluino search with 1 $fb^{-1}$ is sensitive to gluino masses above 1 TeV and the GMSB scenarios with stable stau can be discovered with a few 100 $pb^{-1}$.

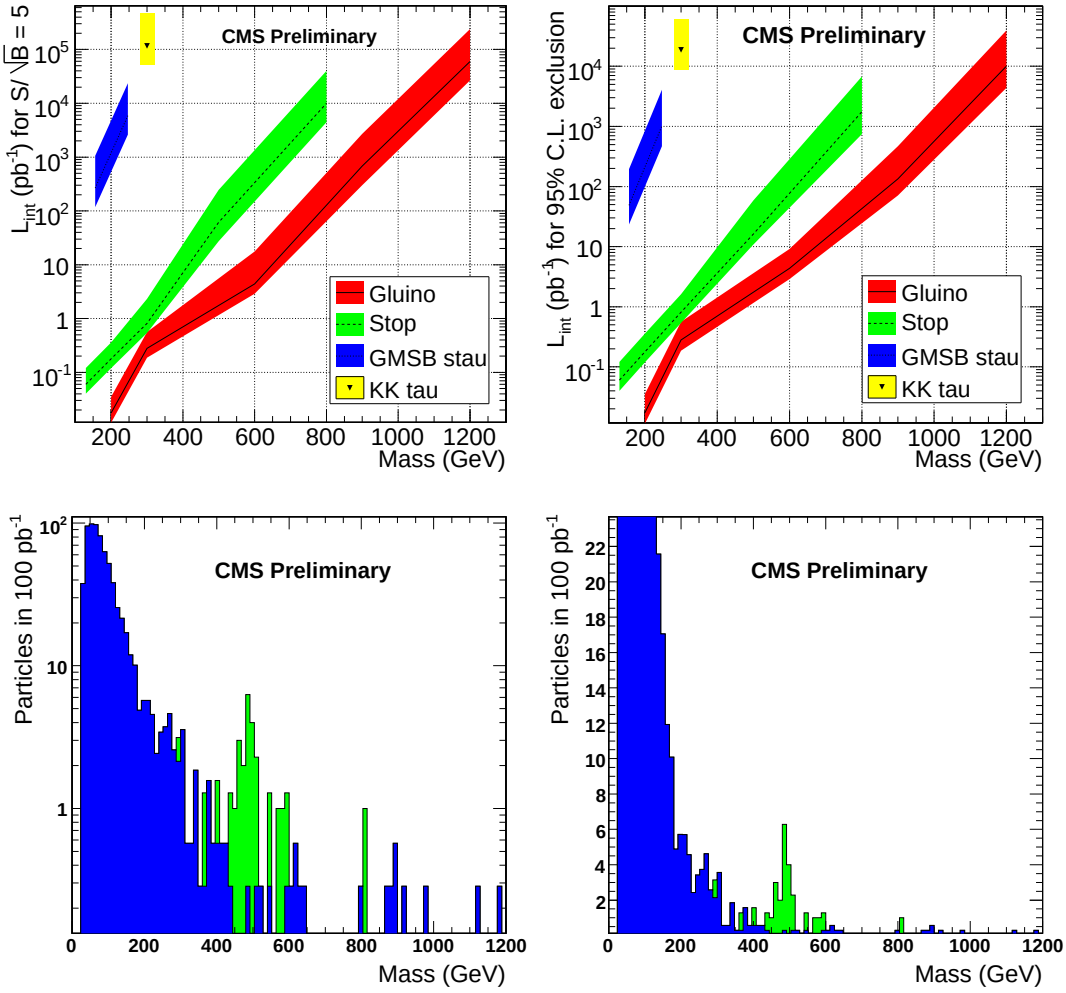


Figure 3: Luminosity needed for discovery (left) or exclusion (right) using the standalone tracker analysis, and reconstructed mass (signal plus background) in 100 pb$^{-1}$ for a 500 GeV $\tilde{t}_1$ (left plot in log scale, right plot in linear scale).

## References

[1] M. Fairbairn et al., Phys. Rept. 438 (2007) 1-63, hepph/0611040.

[2] G.F. Giudice and R. Rattazzi, Phys. Rept. 322 (1999) 419, hepph/9801271.

[3] F.E. Paige et al., hep-ph/0312045.

[4] B.C. Allanach et al., CERN-TH/2002-020, hep-ph/0202233.

[5] T. Appelquist, H. C. Cheng and B. A. Dobrescu, Phys.Rev. D **64**, 035002 (2001)

[6] G. Giudice and A. Romanino, Nucl.Phys. B **699**, 65 (2004).

[7] K. Cheung and W. Y. Keung, Phys. Rev. D **71**, 015015 (2005).

[8] M. Carena et al., Phys. Rev. D66 (2002) 115010, hep-ph/0206167.

[9] R. Barbieri et al., Phys.Rev.D66:095003,2002. hep-ph/0205280.

[10] R.Mackeprang and A.Rizzi, Eur. Phys. J. C **50** (2007) p. 353, hep-ph/0612161

[11] A. C. Kraan, Eur. Phys. J. C **37** (2004) 91, hep-ex/0404001

[12] CMS Collaboration, The European Physical Journal C - Particles and Fields Vol. 46, Num. 3 (June 2006) 605-667.

[13] M.C.Fouz, C.Villanueva, R.Carlin,U.Gasparini,A.T.Meneguzzo,M.Zanetti, G.Cerminara,S.Bolognesi , CMS NOTE-2008/003

[14] A.L. Read, in CERN Report 2000-005, p. 81 (2000)